Influence of grain-boundary defects on electric transport in CeRhSn with a non-Fermi-liquid ground state

A. Ślebarski,[1] K. Szot,[1,2] M. Gamża,[1] H. J. Penkalla,[3] and U. Breuer[4]
[1]*Institute of Physics, University of Silesia, 40-007 Katowice, Poland*
[2]*IFF, Research Centre Jülich, D-52425 Jülich, Germany*
[3]*IWV, Research Centre Jülich, D-52425 Jülich, Germany*
[4]*ZCH, Research Centre Jülich, D-52425 Jülich, Germany*
(Received 11 February 2005; revised manuscript received 25 April 2005; published 18 August 2005; corrected 22 August 2005)

Measurements by atomic force microscopy reported for a polycrystalline CeRhSn sample show nanometer-sized grains consisting of crystalline components. The grains are separated by a grain boundary. The high-resolution electron microscopy and secondary-ion mass spectrometry were used to determine homogeneity of the grains and the grain boundary. The grains are homogeneous up to about 60% of the major phase, with slightly off-stoichiometric phases constituting the balance, whereas the volume fractions of intercrystalline components are strongly inhomogeneous and off stoichiometric. We argue that there is possibly a ballistic transport of electrons through an interface between the grains, which strongly modifies the resistivity of the CeRhSn stoichiometric grains, which is non-Fermi-liquid in character.

DOI: 10.1103/PhysRevB.72.085443 PACS number(s): 61.10.Nz, 71.27.+a, 61.72.Ff, 66.30.Qa

I. INTRODUCTION

The compound CeRhSn exhibits a non-Fermi-liquid (NFL) character of the temperature dependence for low-temperature physical properties.[1] It has been shown that the electrical-resistivity change rises as a function of temperature ($\Delta\rho \propto T^{\varepsilon}$) with exponent $\varepsilon \cong 1$, whereas both the quantity $C(T)/T$ related to the specific heat C, as well as the magnetic susceptibility $\chi(T)$, vary as T^{-n}, with $n \cong 0.5$.[1] There are few scenarios that could explain these anomalous behaviors, e.g., spin fluctuation theory,[2,3] the Kondo disorder model,[4,5] and the Griffiths-McCoy model.[6] Of all the existing theories the Griffiths-McCoy model appears to best describe the observed NFL behavior in CeRhSn.[7] In this model the presence of sufficiently strong disorder and the competition between the Kondo effect and the Ruderman-Kittel-Kasuya-Yosida (RKKY) interaction can lead to small magnetically ordered regions (Griffiths phases[8]), where dynamics may dominate thermodynamic properties of the system in a finite region around a quantum critical point due to tunneling between different configurations. In view of the role of disorder in the formation of the NFL state[9] it is of interest to investigate the microscopic disorder in CeRhSn.

The behavior of local moments in disordered Ce-Rh-Sn alloy has been considered in our past studies.[10] The atomic-sphere approximation by the self-consistent tight-binding linearized muffin-tin orbital method and the local-spin-density approximation yields a magnetic moment $\mu \neq 0$ for the disordered alloys, while the ground state of the CeRhSn compound calculated with atomic order produces a nonmagnetic result. In this framework the presence of disorder in CeRhSn leads to a phase transition to an inhomogeneous ferromagnet ("mictomagnet"),[11] which may be understood as a consequence of magnetic clusters which are formed in the disordered paramagnetic Ce-Rh-Sn alloy.

In this paper we report on the structure and microscopic analysis of CeRhSn, which has revealed nanometer-sized crystalline grains separated by intercrystalline regions. A time-of-flight secondary-ion mass spectrometry (TOF SIMS) analysis in combination with measurements by atomic force microscopy (AFM) has revealed strong chemical inhomogeneity in the grain-boundary space. Chemical inhomogeneity in the grain-boundary space complicates the existing theories that explain the NFL behavior. The grain-boundary size is much smaller than the grain size. Thus, the grain boundary can act as a barrier for the cross transport of the conduction electrons and can be treated as a nanobridge which operates in the ballistic transport regime, where the electron mean free path in the grain exceeds the "constriction" diameter. The electric transport through the barrier should be described by thermally activated behavior, whereas the grains (with atomic disorder) are metallic. Thus, the grain-boundary space in CeRhSn can play an important role in the low-temperature electrical properties. Based on the barrier character of the grain boundaries we discuss the resistivity $\rho(T)$ in the low-temperature range. We suppose that CeRhSn is not the only example of the Ce-based heavy-Fermi intermetallics which can exhibit simultaneously NFL behavior and thermally activated electric transport through the grain-boundary space; however, the problem has not been investigated yet.

II. EXPERIMENTAL DETAILS

Polycrystalline samples of CeRhSn, Ce_xRhSn, and $CeRh_xSn$, where $x=0.95$ or 1.05, were prepared by arc-melting stoichiometric amounts of the elemental metals in an ultrahigh-purity Ar atmosphere and then annealing for 8 days at 800 °C. The samples were examined by x-ray powder diffraction analysis and found to consist of a single phase. The samples were crystallized in a hexagonal unit cell of the Fe_2P type (space group $P\bar{6}2m$). The structure of the samples was first studied by x-ray diffraction (XRD) using Cu $K\alpha$ radiation.

Further insight was gained with a comprehensive transmission electron microscopy (TEM) study. Analytical data collection and selected-area electron-diffraction (SAED) patterns were recorded in a CM 200 FEG microscope operating in the nanoprobe mode (200 kV). A specimen for the high-resolution transmission electron microscopy observation was cut from the bulk sample using a focused ion beam technique. To prepare high-quality TEM cross-section samples of thickness less than 100 nm we used a high-energy Ga^+ beam. The elemental composition on a nanometer scale of the specimen was analyzed with an energy-dispersive x-ray spectrometer (XEDS).

To reveal the different elemental distributions in the surface of CeRhSn we used a time-of-flight secondary-ion mass spectrometry method. An ion Tof IV TOF SIMS (ION-TOF, Münster, Germany) instrument was used. Superior lateral resolution of the liquid metal ion source better than 100 nm allows the analysis of individual microcrystals with a size well below 1 μm.

X-ray photoelectron spectroscopy (XPS) spectra were obtained with monochromatized Al $K\alpha$ radiation at room temperature using a PHI 5700 ESCA spectrometer. The spectra were measured immediately after cleaving the sample in a vacuum of 10^{-10} Torr. Binding energies were referenced to the Fermi level ($\epsilon_F=0$).

The electronic structure of CeRhSn was studied by the self-consistent tight-binding linearized muffin-tin orbital method[12] within the atomic-sphere approximation and the local-spin-density approximation. The exchange-correlation potential was assumed in the form proposed by von Barth and Hedin[13] and Langreth-Mehl-Hu corrections were included.[14] The electronic structure was computed for the experimental lattice parameters for the supercell model. The values of the atomic Wigner-Seitz (WS) sphere radii were chosen in such a way that the sum of all atomic-sphere volumes was equal to the volume of the unit cell.

III. RESULTS AND DISCUSSION

A. Structural characterization

The compound CeRhSn crystallizes in a hexagonal structure. Careful analysis of the x-ray diffraction data, in which the crystal structure was refined with the Rietveld method, revealed the presence of crystallographic disorder. The shape of the reflections does not agree well with the calculations, particularly in the 2θ range of the tail of each line, which could be attributed to small distortions of the lattice resulting from disorder. Thus, first we present the electron diffraction patterns registered in different crystalline grains, and then we analyze the XRD results.

The electron diffraction results confirm the nanometer-sized crystalline grains in CeRhSn with a size of ~200 nm. Figure 1 shows a SAED pattern registered in two different nanoparticles. In Fig. 1(a) we present a SAED pattern which is indexed as the $[1\bar{2}1]$ zone axis of a hexagonal structure with lattice parameters $a=7.241\pm0.166$ Å and $c=3.852\pm0.068$ Å. Figure 1(b) shows an electron diffraction image from a block of ~200 nm consisting of smaller nanocrystalline grains. The investigated grains are oriented in different directions, e.g., the next measured diffraction pattern was indexed in the $[1\bar{1}2]$ zone axis with $a=7.271\pm0.169$ Å and $c=4.453\pm0.150$ Å and another one in the [001] zone axis with $a=7.46\pm0.08$ Å. The composition of these crystalline grains obtained by XEDS is similar and close to the formula $Ce_{35}Rh_{32}Sn_{33}$. We also found intercrystalline regions with an atomic composition drastically different from that expected for the stoichiometric compound (e.g., $Ce_{46}Rh_{24}Sn_{30}$ or $Ce_{29}Rh_{48}Sn_{23}$). The composition of $Ce_{35}Rh_{32}Sn_{33}$ thus obtained for the Ce-Rh-Sn sample is, however, overstoichiometric in Ce by about six parts per 100 compared to the Sn, and worse when compared to the Rh. We therefore also report the XRD results for the off-stoichiometric Ce_xRhSn and

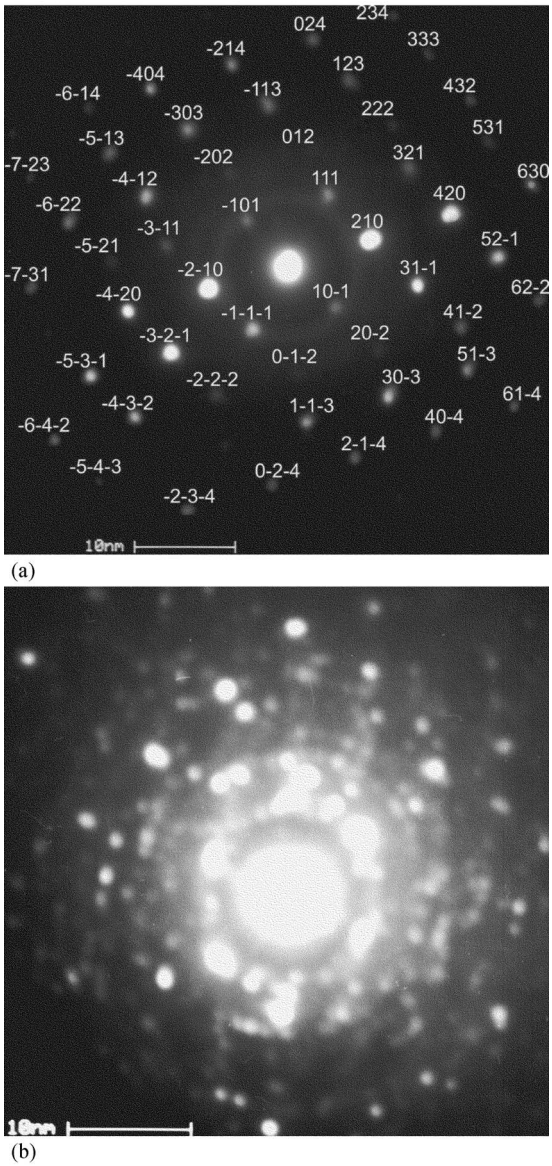

FIG. 1. (a) SAED pattern for nanometric-sized CeRhSn sample (of ~200 nm) indexed in $[1\bar{2}1]$ zone axis with the lattice parameters $a=7.241$ Å and $c=3.852$ Å. (b) Electron diffraction image from the block of ~200 nm which consists of the smaller nanocrystalline grains of CeRhSn.

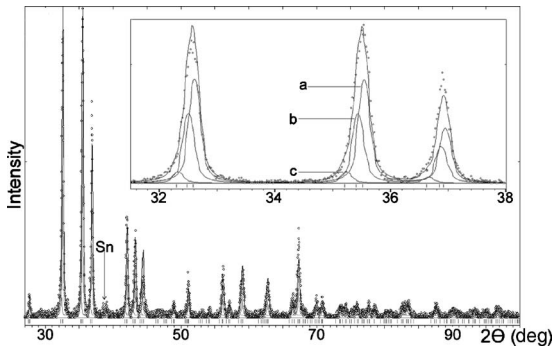

FIG. 2. The observed at $T=13$ K (open points) and calculated (solid line) x-ray diffraction patterns of the hexagonal $CeRh_{0.95}Sn$ sample. The total distribution of the calculated XRD intensities consists of the diffraction spectra calculated for three hypothetical compounds with different lattice constants: phase a, $a=7.433$ Å and $c=4.075$ Å (58%); phase b, $a=7.446$ Å and $c=4.095$ Å (36%); phase c, $a=7.490$ Å and $c=4.115$ Å (6%); see discussion in Sec. III A. Inset: experimental and calculated profiles of (111), (201), and (210) diffraction lines. The XRD pattern of the off-stoihiometry $CeRh_{0.95}Sn$ sample shows a small peak at $2\theta=39$ deg attributed to Sn.

$CeRh_xSn$ ($x=0.95$ and 1.05) samples in which the volume fractions of intercrystalline components arise from the presence of disorder introduced intentionally by the composition (x).

The observed and calculated XRD spectra are given for $CeRh_{0.95}Sn$ (as an example) in Fig. 2. To explain the divergence between the shapes of the XRD lines (in the inset of Fig. 2) we suggest that small off-stoichiometric grains (clusters) with slightly different lattice parameters from those of the homogeneous CeRhSn compound may be distributed throughout the polycrystalline sample. The x-ray diffraction intensities in Fig. 2 obtained at $T=13$ K are well fitted if one takes into consideration a mixture of (minimum) three Ce-Rh-Sn alloys with the lattice parameters $a=7.433$ Å and $c=4.075$ Å (phase a with the volume fraction 58%), $a=7.446$ Å and $c=4.095$ Å (phase b, volume fraction 36%), and $a=7.490$ Å and $c=4.115$ Å (phase c, volume fraction 6%).

We have not obtained the lattice parameters for the off-stoichiometric Ce_xRhSn and $CeRh_xSn$ samples by SAED elemental analysis; however, the thorough analysis of the XRD patterns for CeRhSn as for understoichiometric and overstoichiometric compounds clearly indicates a very similar spread in the lattice parameters as needed to simulate the proper XRD patterns. A random variation in the achieved stoichiometries could be a reason for similar temperature dependences of the lattice parameters, experimentally observed for CeRhSn and the off-stoichiometric compounds (these data are not presented here), and for the indistinguishability of the XPS data across various stoichiometries (see Sec. III B).

B. The morphology of the microstructure

Figures 3(a)–3(d) are XEDS image showing segregation of a Ce-rich fraction in CeRhSn [in Fig. 3(a)] and in

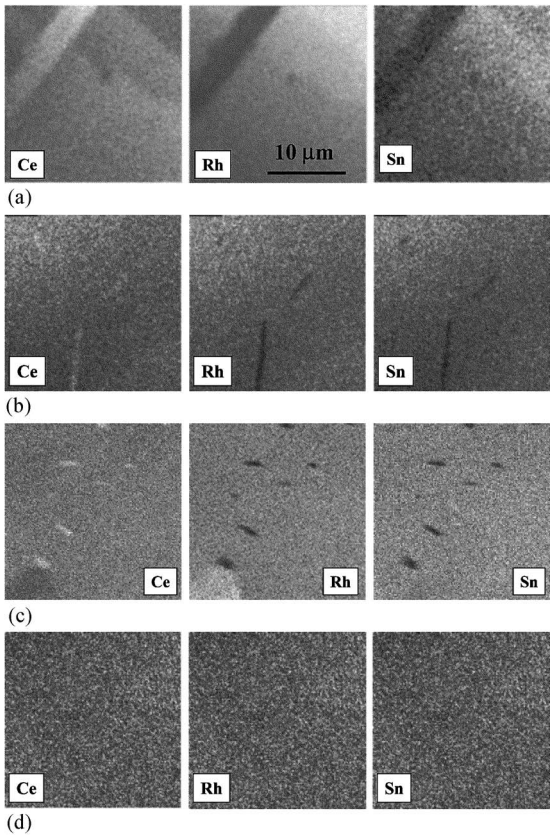

FIG. 3. XEDS micrographs showing segregation of Ce-rich fraction in CeRhSn (a) and $Ce_{1.05}RhSn$ (b) samples. In (c), image shows Rh-rich fraction for $CeRh_{1.05}Sn$ sample. In (d), corresponding XEDS micrographs for $CeRh_{0.95}Sn$ sample.

$Ce_{1.05}RhSn$ [in Fig. 3(b)] samples. In Fig. 3(c) the XEDS image shows disengagement of a Rh-rich volume fraction and small Ce-rich islands. The XEDS image of $CeRh_{0.95}Sn$ shows almost homogeneous distribution of Ce, Rh, and Sn atoms. The results show that the off-stoichiometry intercrystalline fractions evidently deviate from an equilibrium state, i.e., the solid solubility in the grain boundary differs consid-

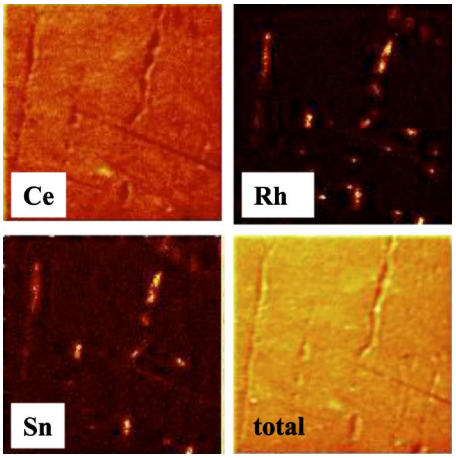

FIG. 4. (Color online) TOF SIMS images for CeRhSn in the analyzed fields of size 97.7×97.7 μm^2.

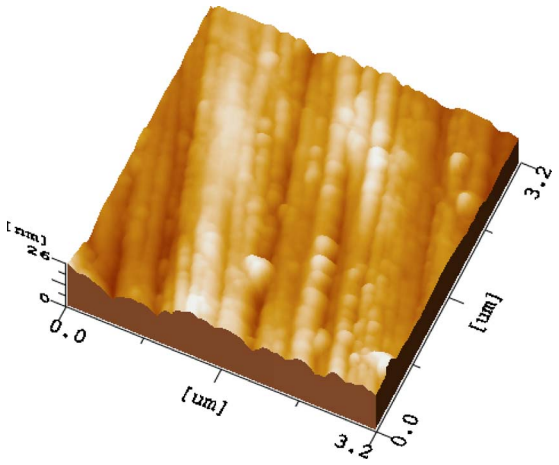

FIG. 5. (Color online) AFM image of the surface of CeRhSn.

erably from that in the interior of the crystals. As a consequence of solute enrichment at the grain boundaries CeRhSn can be classified in the group of nanocrystalline materials.

The XEDS results are in agreement with the results obtained by TOF SIMS. Secondary-ion mass spectroscopy shows the volume fractions of intercrystalline compounds with strong chemical inhomogeneity in the analyzed fields of size $97.7 \times 97.7\ \mu m^2$. Figure 4 is a TOF SIMS image showing separation of elongated Rh-rich intercrystalline regions of the thickness of ~20 nm. These intercrystalline components could play the role of an interface or grain boundary between neighboring crystallites.

C. Atomic force and scanning tunneling microscopy results

In Fig. 5 we present results of AFM measurements for the surface of the CeRhSn sample. The surface showed regular and parallel crystallite wires of variable thickness d ranging from ~0.04 to 0.35 μm. Figure 6 shows the distribution of crystallite size d well described by the Euler Γ function

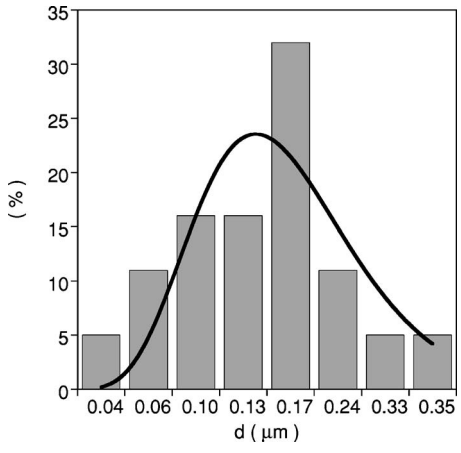

FIG. 6. The number of crystallites (in %) of variable thickness d observed in the field of size $10 \times 10\ \mu m^2$ (presented in Fig. 5), and Euler Γ distribution function (details in Sec. III C). The most probable thickness $d \cong 130$ nm. The Euler Γ distributions obtained from different fields of the sample surface are similar.

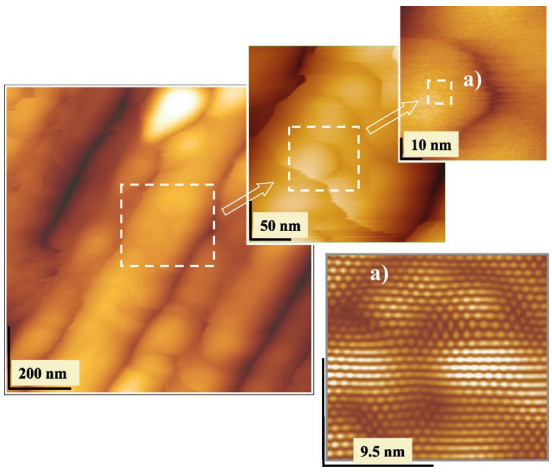

FIG. 7. (Color online) AFM image of surface and STM image from a small part of this surface with atomic resolution. The topography shows dislocations and point defects.

$n(d) = d^{\alpha} e^{-\beta d}$, where $n(d)$ is a number of grains with size d, and $\alpha = 7.01$ and $\beta = 1.64$ are fitting parameters. The most probable thickness $d \cong 130$ nm.

The scanning tunneling microscopy STM experiments, moreover, gave the opportunity to scan the top of the wires with an atomic resolution. As shown in Fig. 7, we even observed the point defects and dislocations which separate the atoms related to the unit cell of CeRhSn. An image is obtained with atomic resolution, to show the atoms in the inset (a) of Fig. 7 we used the fast Fourier transform method.

In Fig. 8 we present an AFM image operating in contact current mode. In this mode simultaneously are measured both the topography and local conductivity of the sample surface. The current in Fig. 8 measured along the line in the AFM contact current mode image (the left upper panel in Fig. 8) exhibits oscillations which can be attributed to the grain-boundary barrier effect. The nanosized grains are metallic and obey Ohm's law ($U = RI$; see Fig. 9).

D. Valence-band XPS spectra

Recently, we have studied the electronic structure of CeRhSn;[1] now we compare the XPS valence-band (VB)

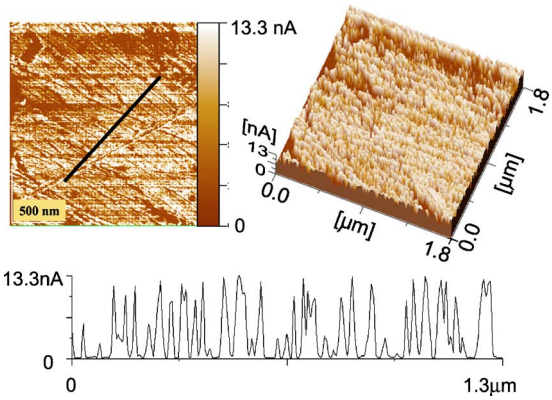

FIG. 8. (Color online) AFM contact current mode image with the local conductivity of the CeRhSn sample. Below, contact current measured along the line shown in AFM contact current image.

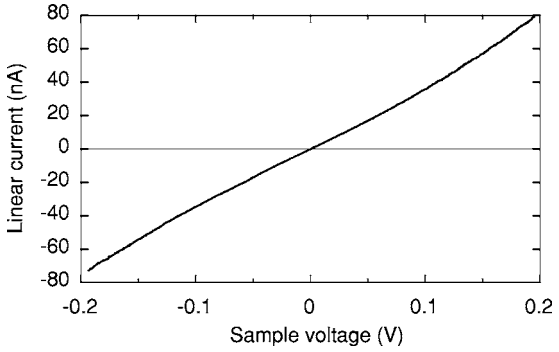

FIG. 9. The contact current measured on CeRhSn vs sample voltage (*I-V* measurement mode) using a conductive cantilever and applying a bias between the tip and sample.

spectra obtained for CeRhSn and for the off-stoichiometry Ce-Rh-Sn samples. Our main goal in this study is to correlate the changes in the morphology of the real surface of CeRhSn with the XPS valence bands. In Fig. 10 are shown the XPS VB spectra of CeRhSn, Ce_xRhSn, and $CeRh_xSn$ ($x=0.95$ and 1.05) and the density of states (DOS) calculated for the stoichiometric CeRhSn compound. The DOSs were multiplied by the corresponding cross sections.[15] A background, calculated by means of a Tougard algorithm,[16] was subtracted from the XPS data. The spectra reveal a valence band that has a major peak mainly due to the *d* states of Rh located near the Fermi level. The second peak at ~7 eV is due to the Sn *s* states. All XPS VB spectra presented in Fig. 10 are similar, and do not show clear evidence for a local chemical decomposition influence on their shape.

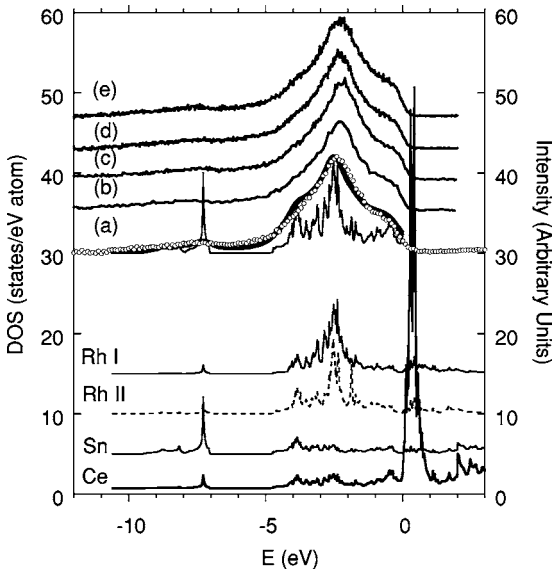

FIG. 10. In (a), comparison of the total DOS calculated for CeRhSn (thin curve) convolved with Lorentzians of half-width 0.4 eV, taking into account proper cross sections for bands with different *l* symmetry (thick curve), and the measured XPS valence bands for CeRhSn (open points, curve *a*), $Ce_{0.95}RhSn$ (curve *b*), $Ce_{1.05}RhSn$ (curve *c*), $CeRh_{0.95}Sn$ (curve *d*), and $CeRh_{1.05}Sn$ (curve *e*), respectively, corrected by the background. The partial DOS curves are plotted below.

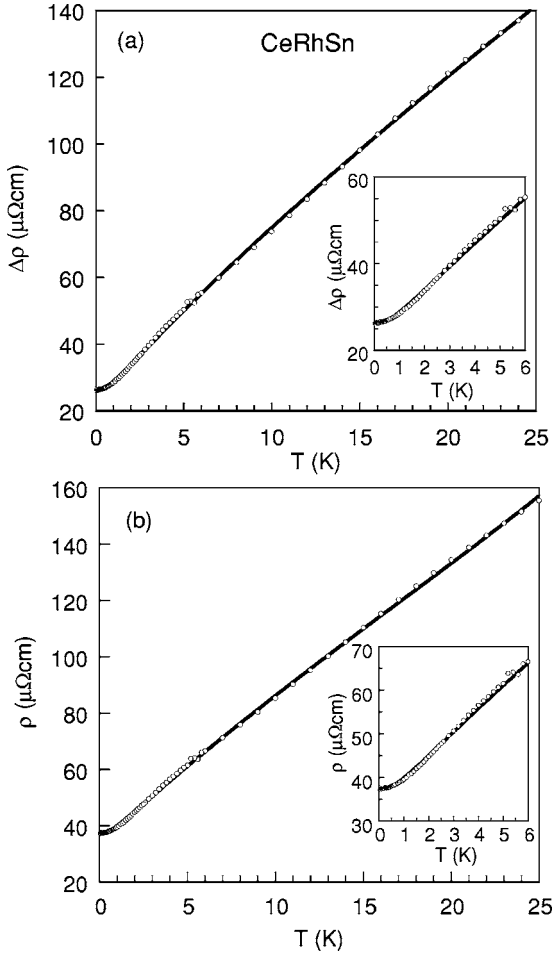

FIG. 11. (a) Incremental electrical resistivity $\Delta\rho=\rho(\text{CeRhSn})-\rho(\text{LaRhSn})$ versus temperature T (after Ref. 7) and fit of the expression $\Delta\rho(T)=AT^{\varepsilon}+B\exp[\Delta/(T+\theta)]$ to the resistivity data (details in Sec. IV). Shown in the inset is a plot of $\Delta\rho$ versus T of CeRhSn and the fit between 0.1 and 6 K. (b) The as-measured resistivity ρ for CeRhSn fitted to a $\rho(T)=\rho(0)+\alpha T^5+AT^{\varepsilon}+B\exp[\Delta/(T+\theta)]$ dependence. The $\rho(0)$ and α parameters are obtained from the $\rho(T)$ data for LaRhSn, which exhibits T^5 behavior below 25 K. The inset shows ρ versus T of CeRhSn and the fit below 6 K.

IV. PHYSICAL DISCUSSION

Microanalysis in combination with x-ray diffraction has revealed that CeRhSn is a type of nanocrystalline material; it contains nanometer-sized crystalline grains in the shape of wires separated by the grain-boundary space with strong chemical inhomogeneity. The grain boundary or interface between neighboring crystallites (grains) is very important in controlling the macroscopic properties of the sample. It acts as barrier for the cross transport of the carriers, as is shown in Fig. 8. When an electron mean free path (in grains) exceeds the grain-boundary size, there is possible ballistic transport through the barrier, while in the grain the resistivity is indeed NFL in character. This assumption seems to be the relevant scenario for CeRhSn. The AFM studies and microanalysis provide some support for this model.

Our systematic studies of CeRhSn have shown clear evidence for the NFL behavior.[1] The susceptibility χ and spe-

cific heat C divided by temperature, C/T, in a CeRhSn sample can be fitted to T^{-n} behavior at low temperatures.[7] The values of the power-law exponent $n \cong 0.5$ obtained from the $C(T)$ and $\chi(T)$ data are in agreement within experimental resolution, suggesting that the NFL behavior can be described by the Griffiths-McCoy model. Also, the resistivity shows a nearly linear temperature dependence over a wide range down to 3 K; however, between 0.1 and 3 K $\rho(T)$ displays a $T^{1.7}$ temperature scaling. The resistivity is indeed NFL in character; however, the power-law divergence in temperature, which extends over several decades in temperature, has not been understood. The assumption of the ballistic electron transport through the barrier provides the following simple picture. It is assumed that the resistivity of CeRhSn has a power-law temperature dependence consistent with NFL behavior in each grain, and an activated behavior between grains varying as $\exp[\Delta/(T+\theta)]$. As illustrated in Fig. 11, we find that the equation $\Delta\rho(T)=AT^{\varepsilon}+B\exp[\Delta/(T+\theta)]$ fits the ρ data successfully in the whole temperature range, i.e., between 0.1 and 25 K, if $A=8.44$ $\mu\Omega$ cm, $B=16.29$ $\mu\Omega$ cm, $\varepsilon=0.84$, $\Delta=0.42$ K, and $\theta=0.88$ K. $T+\theta \equiv T_d$ is understood as a "defect temperature" in analogy to electromigration processes in metal nanobridges (T_d is discussed, e.g., in Ref. 17). The T dependence of the resistivity increment $\Delta\rho(T)$ of CeRhSn is determined by subtracting the lattice contribution of LaRhSn, on condition that the sample of LaRhSn is free from the types of disorder that lead to, e.g., the excitation-like contribution used in the $\Delta\rho$ fitting function. Thus, to exclude the possibility that subtraction of the background contribution to $\rho(T)$ can generate both the NFL exponent and activated behavior seen in the incremental resistivity $\Delta\rho(T)$, first we analyzed ρ of LaRhSn, which is consistent with the expression $\rho(T)=\rho(0)+\alpha T^5$ in the range $T<25$ K, which is characteristic of metals. Then, the as-measured $\rho(T)$ for CeRhSn was fitted with a function that combines a generic phonon-electron scattering contribution (i.e., grain-boundary-free) and the postulated temperature variations for $\Delta\rho$. The best fit yields the parameters $A=8.12$ $\mu\Omega$ cm, $B=16.57$ $\mu\Omega$ cm, $\varepsilon=0.85$, $\Delta=0.40$ K, and $\theta=0.90$ K, which are almost the same as those obtained from the $\Delta\rho$ fitting function to the $\Delta\rho$ data (see Fig. 11), indicating that LaRhSn is a good reference material for subtracting the lattice contribution to $\rho(T)$ at low temperatures.

We realize that AFM contact current mode image in Fig. 8 also shows the oxygen defects and oxides absorbed on the surface, which can produce additional interfaces. The presence of oxides within the near-surface region reflects a real contact between an electrode and the sample when the resistivity is measured; however, it does not change markedly the temperature dependence of the electric resistivity.

V. CONCLUSIONS

In summary, our results give evidence for nanometer-sized grains in CeRhSn, separated by a grain-boundary space or interface with strong chemical inhomogeneity. We suggest that the grains which exhibit an atomic disorder are metallic with a non-Fermi-liquid temperature dependence of electrical resistivity; however, the exponent ε depends on the temperature range of fitting the expression $\rho \propto T^{\varepsilon}$ to the $\rho(T)$ experimental data; $\varepsilon \cong 1$ for $T>3$ K, while $\varepsilon=1.7$ below 3 K. The assumption that the electric transport in an interface is ballistic, whereas inside the grain $\rho \propto T$, leads to a qualitative description of the temperature dependence of the electrical resistivity in a wide T range (we obtained a good fit to the ρ data between 0.1 and 25 K).

ACKNOWLEDGMENT

Two of the authors (A.Ś. and M.G.) acknowledge the support of the State Committee for Scientific Research (KBN), through Grant No. 1 P03B 052 28.

[1] A. Ślebarski, A. Jezierski, M. B. Maple, and A. Zygmunt, Acta Phys. Pol. B **32**, 3331 (2001); A. Ślebarski, M. B. Maple, E. J. Freeman, C. Sirvent, M. Radłowska, A. Jezierski, E. Granado, Q. Huang, and J. W. Lynn, Philos. Mag. B **82**, 943 (2002).

[2] A. J. Millis, Phys. Rev. B **48**, 7183 (1993).

[3] T. Moriya and T. Takimoto, J. Phys. Soc. Jpn. **64**, 960 (1995).

[4] O. O. Bernal, D. E. MacLaughlin, H. G. Lukefahr, and B. Andraka, Phys. Rev. Lett. **75**, 2023 (1995).

[5] E. Miranda, V. Dobrosavljevic, and G. Kotliar, J. Phys.: Condens. Matter **8**, 9871 (1996).

[6] A. H. Castro Neto, G. Castilla, and B. A. Jones, Phys. Rev. Lett. **81**, 3531 (1998).

[7] P.-C. Ho, V. S. Zapf, A. Ślebarski, and M. B. Maple, Philos. Mag. **84**, 2119 (2004).

[8] R. B. Griffiths, Phys. Rev. Lett. **23**, 17 (1969).

[9] If disorder were not present there are two possibilities: (i) the compound has long-range magnetic order if the RKKY interaction predominates over the Kondo interaction, (ii) if the Kondo interaction is sufficiently large, the hybridization between the localized f-electron and the $5d$-$6s$ conduction states can lead to the formation of a coherent heavy-Fermi liquid or to gap formation at the Fermi energy (ϵ_F) when temperature $T \to 0$. In both cases the compound will be paramagnetic due to the quenching of the magnetic moments.

[10] A. Ślebarski, M. Radłowska, T. Zawada, M. B. Maple, A. Jezierski, and A. Zygmunt, Phys. Rev. B **66**, 104434 (2002).

[11] A. Ślebarski, K. Grube, R. Lortz, C. Meingast, and H. v. Löhneysen, J. Magn. Magn. Mater. **272-276**, 234 (2004).

[12] O. K. Andersen and O. Jepsen, Phys. Rev. Lett. **53**, 2571 (1984); O. K. Andersen, O. Jepsen, and M. Sob, in *Electronic Structure and Its Applications*, edited by M. Yussouff (Springer, Berlin, 1987), p. 2.

[13] U. von Barth and L. Hedin, J. Phys. C **5**, 1629 (1972).

[14] C. D. Hu and D. C. Langreth, Phys. Scr. **32**, 391 (1985).

[15] J. J. Yeh and I. Lindau, At. Data Nucl. Data Tables **32**, 1 (1985).

[16] S. Tougaard and P. Sigmund, Phys. Rev. B **25**, 4452 (1982).

[17] K. S. Ralls, D. C. Ralph, and R. A. Buhrman, Phys. Rev. B **40**, 11561 (1989).